International Journal of Electrical Components and Energy Conversion
2018; 4(1): 13-20
http://www.sciencepublishinggroup.com/j/ijecec
doi: 10.11648/j.ijecec.20180401.12
ISSN: 2469-8040 (Print); ISSN: 2469-8059 (Online)

Effect of Annealing on the Structural and Magnetic Properties of 3% Sm Doped ZnO

Hanan Hassan Hantour*, Nadia Abd El-Mohsen, Suzan Naser El-Sayed, Assma Mahmoud Aoud Mahmoud

Physics Department, Faculty of Science, Al-Azhar University (Girls), Cairo, Egypt

Email address:
hananhantourmy@yahoo.com (H. H. Hantour)

*Corresponding author

To cite this article:
Hanan Hassan Hantour, Nadia Abd El-Mohsen, Suzan Naser El-Sayed, Assma Mahmoud Aoud Mahmoud. Effect of Annealing on the Structural and Magnetic Properties of 3% Sm Doped ZnO. *International Journal of Electrical Components and Energy Conversion.* Vol. 4, No. 1, 2018, pp. 13-20. doi: 10.11648/j.ijecec.20180401.12

Received: December 28, 2017; **Accepted**: January 30, 2018; **Published**: February 26, 2018

Abstract: The present study focuses on the structural and magnetic properties of Sm doped ZnO at 3% concentrations. These compounds have been synthesized by a chemical coprecipitation method and characterized by X-ray diffraction (XRD), scanning electron microscopy (SEM), transmission electron microscopy (TEM) and magnetization method (M– H). The XRD pattern of all the samples showed ZnO hexagonal wurtzite structure with sharp and intense peaks with small change in lattice parameters due to Sm doping in ZnO, indicating the substitution of Sm ion for Zn sites. Magnetic measurements show an enhancement in room temperature ferromagnetism (RTFM) with Sm doping. Ferromagnetic behavior exists over and above the diamagnetic behavior, RTFM related to The Zn vacancies and diamagnetic (which exists over alarge scale) related to the oxygen vacancies which mediate the interaction of dopant ions.

Keywords: ZnO, Nanoparticles, Semiconductors, Magnetic Materials, Zinc Vacancy, Structure, Microstructure, Magnetic with Different Temperature

1. Introduction

ZnO due to its wide direct band-gap (3.37 eV), large exciton energy (60 meV), chemical and thermal stability as well as low toxicity is considered to have important properties in basic and applied researches [1-5]. Oxide semiconductor based diluted magnetic semiconductor (DSM) is one of spintronic materials, which has both semiconductor and magnetic behavior. The magnetic property from the realization of spin functions [6, 7]. The introduction of impurity atoms into semiconducting materials is the primary method for controlling the properties of the semiconductor, such as band gap or electrical conductivity [8]. Doping is the most effective and efficient way to tune the selectivity of the diluted magnetic semiconductors [9]. Correspondingly, several theoretical models have been developed to explain the coupling mechanism of the magnetic behavior of the samples [10]. The modification of ZnO properties by doping has become an important research topic in order to improve the intrinsic characteristics of the these materials. Doping of ZnO allows it's optical and magnetic properties to be adapted, through alteration of its electronic structure and band gap [11]. In general, ZnO has well separated valence and conduction band. Optical excitation will induce electron–hole pairs where the excitons will form just below the conduction band. These excitons are sensitive to physical and chemical environment in ZnO structure as well as to the presence of defects and dopant.

TM doped ZnO, TM ion interactions play a vital role in controlling the excitation dynamics [12-14], and also, the magnetism is so weak that it is often buried by experimental artifacts and always has the problems of reproducibility or precipitation of secondary metallic phases. Compared with 3d transition metals, 4f rare earth (RE) elements have larger magnetic moments and likely to potentially enhance the ferromagnetism (FM) in doped semiconductors [15, 16]. Theoretical investigations revealed stable FM coupling between RE ions are mediated by the delocalized electrons. This is particularly beneficial to ZnO, since it exhibits n-type conductivity with a large population of's' electrons [17]. The

influence of RE doping in ZnO mainly focus on its optical properties. Few reports are available on RE doped ZnO nanoparticles which provide information about the density of RE ions and also the response of the nanoparticles to the applied magnetic field.

2. Experimental

Samples of ZnO and ZnO:Sm doped have been prepared by chemical coprecipitation by mixing an appropriate amount of NaOH, $ZnCl_2$ and $SmCl_2$ prepare ZnO nanoparticle, 0.5M aqueous solution of $ZnCl_2$ and 1M of NaOH were prepared in deionized water. The method for the preparation of ZnO nanoparticle is a slight modified method of Abdolmajid et al [18]. 1M of NaOH solution was taken in a beaker and heated to 50°C. After 5 mintes of heating the NaOH solution, $ZnCl_2$ was added dropwise to the above heated solution under high magnetic stirring. After the complete addition of $ZnCl_2$, the beaker was sealed and kept at stirring condition for 10 min at 50°C. The white precipitate formation was observed at above conditions [19]. The precipitation was collected and washedwith deionized water and with 100% ethanol then air dried at 100°C. The annealed samples are heated at 400 and 800°C for three hours. The X-ray diffraction, using Philips diffractometer (X'pert MPD) goniometer type PW3050/10 with Cu-Kα radiation source (λ =1.54178 Å); the field emission scanning electron microscopy (FESEM) was performed on JEOL JSM-6700F to investigate the surface morphology of the samples. The Vibrating sample magnetometer (VSM) was used to measure the magnetization curve (M–H) at room temperature. To obtain information on oxidation state and site occupancy of the Sm and Li ions in the ZnO matrix electron spin resonance (ESR) was carried out using X-band JEOL JES-RE1X at room temperature.

3. Results and Discussion

3.1. Structure and Microstructure Analysis

3.1.1. XRD Analysis

Figure 1 indicate The XRD patterns of the ZnO and ZnO doped with 3% Sm at room temperature and annealing temperature 400^0C and 800^0C. Sharp and intense peaks corresponding to the hexagonal wurtzite structure of ZnO with $P6_3mc$ as space group were observed. The sharp peaks indicate that the ZnO: Sm possesses a crystalline structure. It may be noted that all peaks of wurtzite ZnO have their preferred orientation along the (1 0 1) reflection plane for each composition. The comparison of peak positions with the Standard Joint Committee for Powder Diffraction pattern (JCPDS card no. 36-1451) suggests the polycrystalline nature of the system. All the patterns are identified to be a single phase ZnO with hexagonal structure for all compossions at RT, annealed at 400°C and annealing at 800°C. So Sm ion is completely doped into the Zn lattice. Table1 gives the refined structural parameters obtained from Rietveld analysis applying the MAUD program.

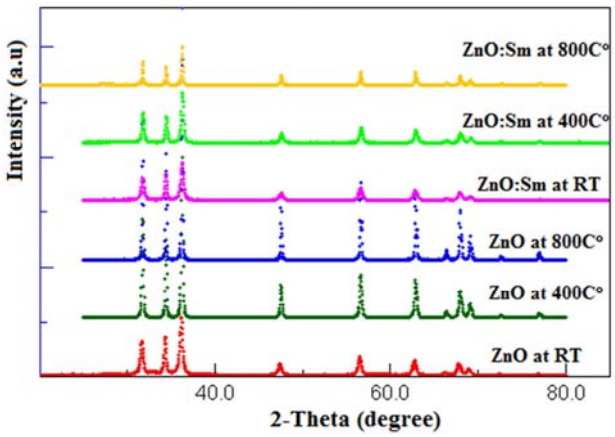

Figure 1. *Diffraction pattern of ZnO and ZnO:Sm systems at: (a) Room temperature (RT), (b) 400°C and (c) 800°C.*

Figure 2 (a, b) illustrate the diffraction patterns fitting resulting from Rietveld analysis of all the compositions at RM (room temperature). During analysis, the site 2b (⅓⅔0) occupancy shared by Zn and Sm, the Sm ion is incorporated substitutionally in the ZnO lattice replacing the Zn ions in the position 2b. The lattice parameters increase with increasing the percentage of Sm where the atomic radius of Sm 2.59 A° is greater than the atomic radius of Zn 1.53 A°. Similar c-axis variations have also been reported in Er, Sm, and Ce doped ZnO. This variation in the lattice parameters occurs due to substitution of the bigger ionic radii of Sm^{3+} (0.964 nm) in place of Zn^{2+} (0.74 nm).

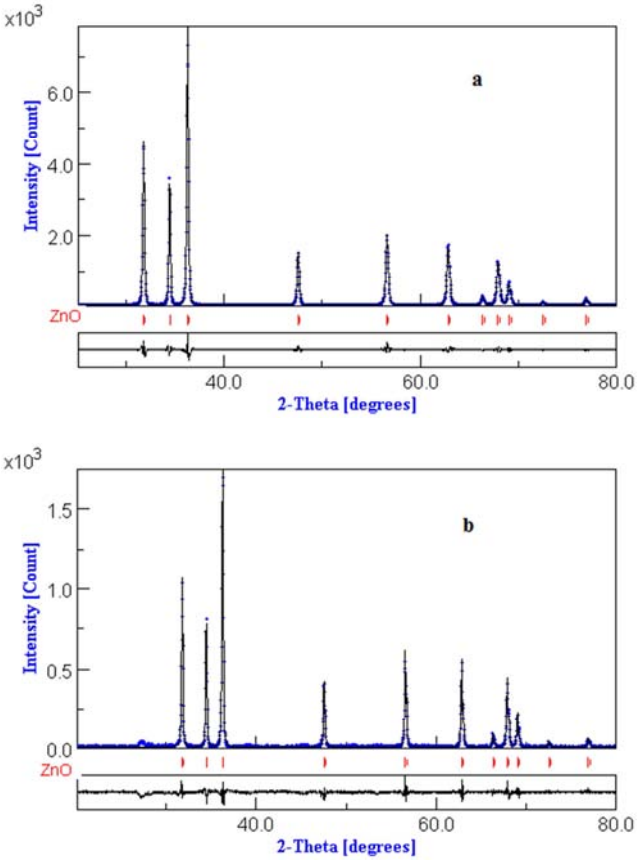

Figure 2. *Profile fitting of: (a) ZnO and (b) $Zn_{0.97}Sm_{0.03}O$.*

The change in the lattice parameter trend reverses with Sm doping which may be associated with the increase in the number of defects due to the substitutional doping of Sm. The parameters a and c depend upon certain factors such as: (i) the concentration of impurity atoms, defects, and the difference between the ionic radii of Zn^{2+} and the impurity atoms Sm; (ii) external strains developed due to external pressures and temperatures. Thus the reduction in the intensity of the peaks and the change in the lattice parameters is associated with the lattice distortion and strain induced in ZnO due to the substitution of Zn^{2+} by Sm^3. An appreciable broadening has also been observed in the XRD peaks, along with the crystallite size, lattice strain also contributes to the broadening of the XRD peaks and has been estimated. This strain induced may be due to a change in the lattice parameters with Sm doping.

The information on strain and crystallite size was obtained from Winfit program the crystallites size which is increas with Sm shown in table1. The internal tetrahedral distortion and the spontaneous polarization in ZnO can be assessed using the atomic position parameter (u), the nearest neighbor bond length along c direction (b) and the bond angles α and β are average basal bond length (O_a-Zn-O_b) and average base apex angle (O_b-Zn-O_b) respectively where O_a refers O atom at the apex and O_b represents O atom at the base of the tetrahedral structure.

Table 1. *The refined lattice parameters (a and c) (A°), average Zn–O bond lengths (b A°), average bond angle, crystallite size (L nm) and mean square strain (ε) obtained from Rietveld analysis of ZnO and ZnO:Sm at RT.*

Parameter	At RT		At 400°C	
	ZnO	$Zn_{0.97}Sm_{0.03}O$	ZnO	$Zn_{0.97}Sm_{0.03}O$
a	3.242	3.2445	3.243	3.244
c	5.192	5.195	5.193	5.195
R_W%	8.236	10.910	6.891	10.268
R_{exp}%	7.528	9.327	4.749	9.313
u	0.3802	0.3798	0.3802	0.3798
b Å	1.985	1.984	1.985	1.984
α	108.364	108.446	108.364	108.446
β	110.555	110.476	110.555	110.476
L (nm)	14.1	13.3	29.9	22.3
ε x 10^{-3}	1.28	1.32	1.32	1.36

3.1.2. Scanning Electron Microscopy (SEM) and High Resolution Transmission Electron Microscopy (HRTEM)

Figure 3 shows The SEM images show surface morphologies of the $Zn_{1-x-y}Sm_xLi_yO$ samples at RT and annealed at 800°C. As it follows from the SEM micrographs the synthesized samples consisted of spherical clusters but these images clearly show that the samples annealed at 800°C is more homogenous in shape and size than the samples at RT. Results obtained by high resolution transmission electronmicroscopy (HRTEM) are shown in Figure 4, 5, 6. The selected area electron diffraction (SAED) image is shown in Figure 4 these patterns suggest that the ZnO and doped powder is in crystalline wurtzite structure as revealed by the XRD study. The HRTEM micrographs in Figure 5 characterized the surface morphology of the samples. It is obvious that these samples are consisting of very good crystallized areas of nanosized. The interlayer spacing d=0.2 nm of the all samples corresponding to the (1 0 1) plane. The morphologies are shown in Figure 6. The particle sizes are mainly between 25-66 nm, the average crystallite sizes of the samples determined by X-ray diffraction were significantly smaller than the values determined by TEM, which can be attributed to the fact that the values observed by TEM have the size of the secondary particles. In addition, the X-ray line broadening analys is disclosed only the size of a single crystallite.

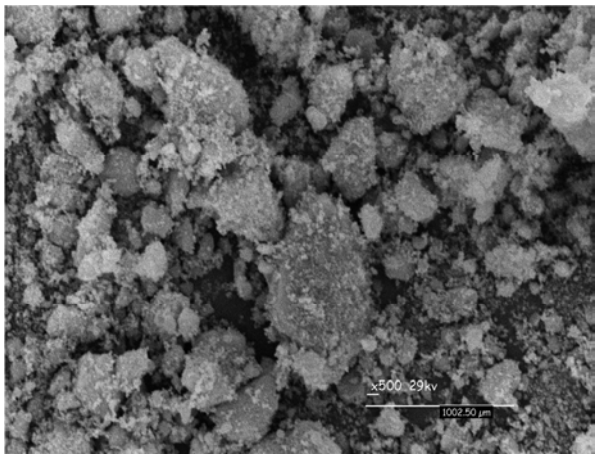

ZnO at RM

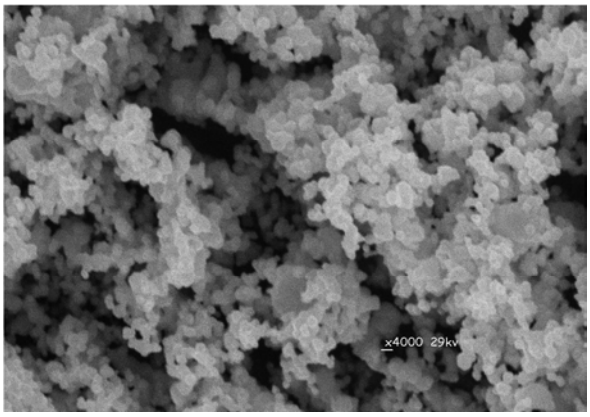

ZnO at 800^0C

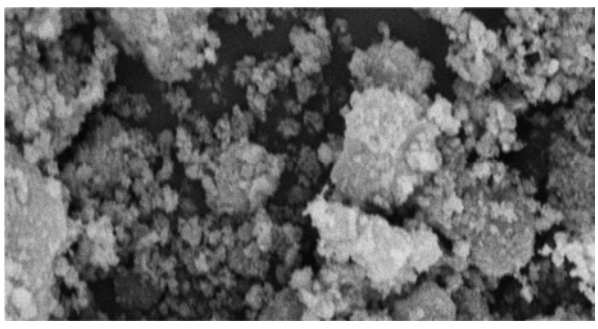

$Zn_{0.96}Sm_{0.03}$ O at RM

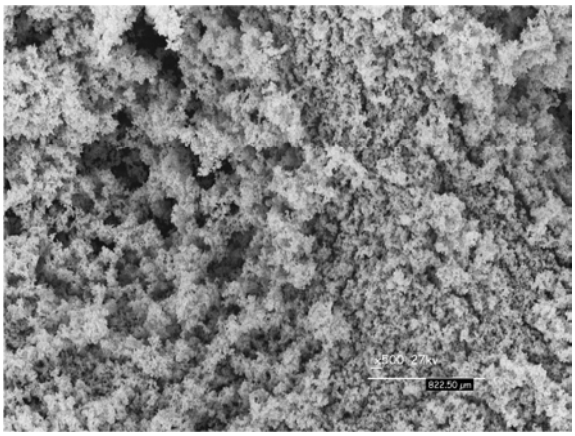

$Zn_{0.96}Sm_{0.03}$ O at 800°C

Figure 3. *SEM of Zn0.96Sm0.03 systems annealing at RT and 800°C.*

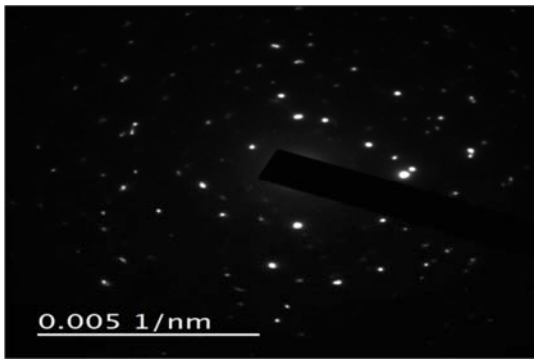

ZnO

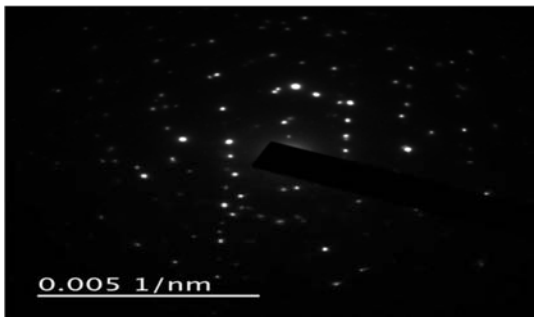

$Zn_{0.97}Sm_{0.03}O$

Figure 4. *The selected area electron diffraction (SAED) of Zn0.96Sm0.03 systems.*

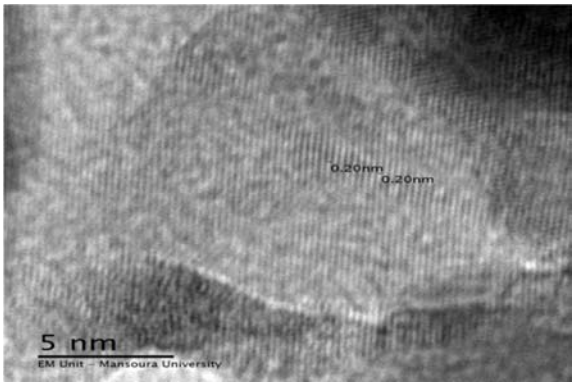

ZnO

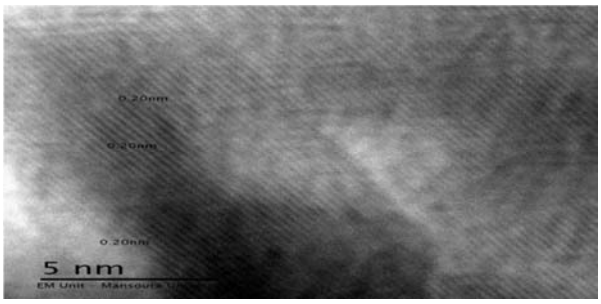

$Zn_{0.97}Sm_{0.03}O$

Figure 5. *High resolution TEM of Zn0.96Sm0.03 system.*

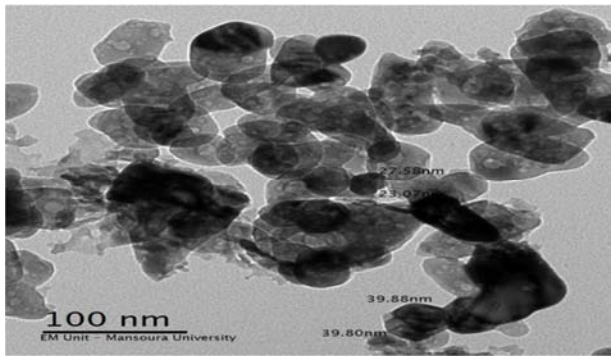

ZnO

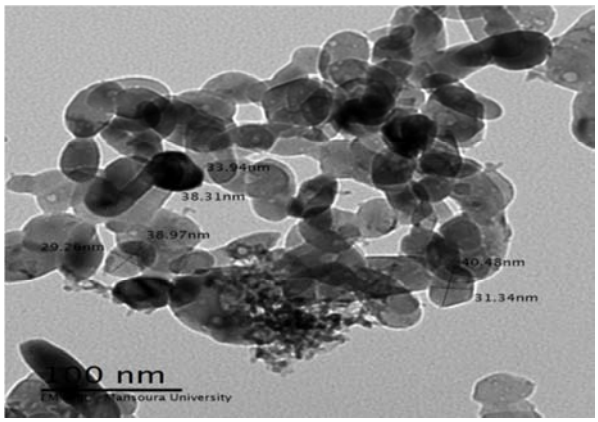

$Zn_{0.96}Sm_{0.03}$ O

Figure 6. *Transmission electron micrograph of Zn0.96Sm0.03 system.*

3.2. Magnetic Studies

3.2.1. VSM Characteristic

Figure 7 shows dc magnetization hysteresis loop of pure ZnO measured at RT. It is observed that ZnO nano particles exhibit a ferromagnetic behavior with coercivity (H_C) of 286 Oe, saturation magnetization (M_S) of 0.973 emu/g and remnant magnetization (M_R) = 0.199 emu/g. Some groups have also reported ferromagnetism in pure ZnO nano particles and thin films [20-26]. They intend that ferromagnetism is the universal feature of the nano particles of non-magnetic oxides. They explained that the origin of ferromagnetism in these nanoparticles is due to oxygen vacancies. But recently, some theoretical group has reported that ferromagnetism in ZnO is due to the Zn vacancies and suggested that the origin of the magnetism does not result

from the Zn 3d electron but it is originated from the unpaired 2p electron of O atom in the immediate vicinity of Zn vacancies [24, 27]. Zubiaga et al [28] study defect in ZnO bulk using positron annihilation life time spectroscopy and reported the presence of Zn vacancies in pure ZnO. Therefore, the RTFM in pure ZnO rods are due to the Zn vacancies induced spin polarization [26].

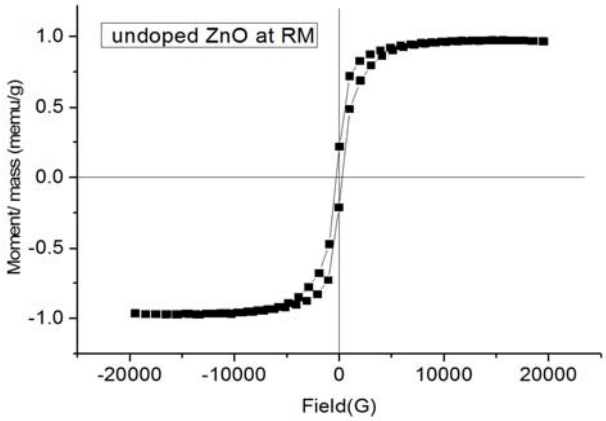

Figure 7. *Hysteresis loop of pure ZnO measured at RT.*

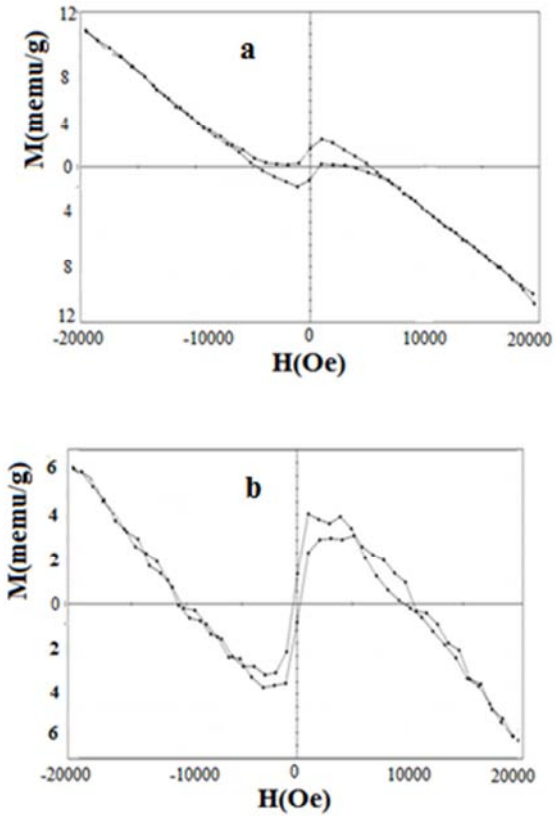

Figure 8. *Hysteresis loop of pure ZnO annealed (a) at 400°C and (b)at 800°C.*

After annealing at 400°C and 800°C the undoped ZnO sample shows weak ferromagnetic behavior and the values of H_C, M_S and M_R are decreased with increase in the annealing temperature as shown in Figure 8a, b. With annealing at 400°C H_C= 990 Oe, M_s=2.33x10^{-3}emu/g and M_R=1.616x10^{-3}emu/g and at 800°C H_C=312 Oe, M_s=3.643x10^{-3} emu/g and M_R=1.11x10^{-3} emu/g. Quite a few reports [29-31] indicate occurrence of ferromagnetic ordering in nanocrystals of nonmagnetic solids and ions [29] (Zn^{2+} and O^{2-}) due to surface defects. Although there is a possibility of presence of Zn interstials and oxygen vacancies at surface of undoped ZnO nanocrystals, these defects are not large enough to induce ferromagnetism in undoped ZnO nanocrystals [30].

In bound magnetic polarons (BMP) model, the oxygen vacancy as defect mediates the spins of localized electrons of dopant ions in 3d state, but the mechanism of FM in pure ZnO without magnetic ions is not clear. Here, we give simple approach; we believe that the magnetism of undoped ZnO should be coming from the change in the net spins in the d orbits of Zn ($3d^{10}$). The d-orbits should be uncompleted with unpaired electron ($3d^9$) which may be achieved by defects like oxygen vacancy (V_O). The V_O may capture one electron from the complete field-band of Zn (d^{10}) to be uncompleted filled d-orbits that leads to a net spin one-half in Zn orbits, for stabilization of the system. The magnetic decrease with increase in the annealing temperature. This is directly related to the decrease in V_O concentration [32].

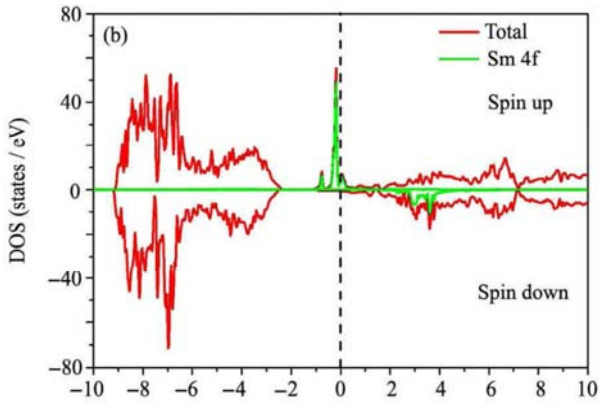

Figure 9. *The total DOS of the super cell contains a Sm_{Zn}[37].*

When we replace one Zn atom with Sm, and the calculations suggest that one Sm substitutional (Sm_{Zn}) favors the ferromagnetic ground state with an energy difference of E_{AFM}-E_{FM} =296 meV and the total magnetic moment is 0.337 μB. Systems with a single zinc vacancy, oxygen interstitial are magnetic as well with moments of 1.75 μB and 1.99 μB, respectively [33]. Abundant Reports have shown that the obtained magnetism in V_{Zn} and O_i originates from the p orbitals of the oxygen atoms around the defect sites via p-p exchange interaction [34-36]. The total DOS of the super cell contains a Sm_{Zn} is illustrated in Figure 9 [37]. For ZnO:Sm the 4f electrons occupy gradually the majority spin t_{1g} states, majority spin t_{2g} states and majority spin a_{2g} states, thus the total magnetic moment increases. The 4f electrons in the majority spin states are totally occupied, and the Fermi level shifts into the conduction band, the electrons occupy gradually the minority spin t_{1g} states, t_{2g} states and a_{2g} states, then the total magnetic moment decreases as shown in Figure 10. Indeed, the 4f states show a large spin exchange splitting ε_d, i.e.: the energy difference between the centers of majority

spin and minority spin states and a small crystal field splitting, i.e.: the energy difference between t_{1g} and a_{2g} states for one kind of spin. Moreover, the exchange splitting ε_d is in an increasing order for the rare earth elements, and the crystal field splitting of the majority spin states decreases as the number of 4f electrons increases [37].

Detailed magnetic measurements were carried out on undoped as well as 3% Sm doped ZnO samples at room temperature with a vibrating sample magnetometer. The magnetization characteristics of the samples are shown in Figure10. Whereas undoped ZnO showed ferromagnetic behavior the characteristics start changing with doping of Sm^{3+} in ZnO. With Sm 3% doping, a ferromagnetic loop is seen in the magnetic field region of −6000 to 6000 Gauss over and above the diamagnetic trend as shown in Figure 10. The ferromagnetic behavior is increase with increase annealing temperature at 400°C and then decrease with increase the annealing temperature at 800°C. Experimental observation of existence of ferromagnetism in ZnO lattice solely due to Sm doping confirms the magnetic ordering at room temperature in ZnO:Sm nanocrystals [38]. As XRD indicate formation of one phase in ZnO:Sm samples with change in 'a' and 'c' lattice parameters and does not show any precipitated phase, it can be inferred that Sm is incorporated into ZnO lattice in Zn substitutional site. Thus observed change in magnetic behavior is occurring solely due to Sm incorporation in ZnO lattice. The observed magnetism at room temperature in rare earth Sm^{3+} doped ZnO has its origin in magnetic interaction between Sm^{3+} ions and is intrinsic in nature. The observations strongly suggest that a room temperature diluted magnetic semiconducting oxide has been realized in Sm doped ZnO. Dilute ferromagnetism has been observed in undoped ZnO [31], transition metal doped ZnO [39-44] and Li/Na doped ZnO [45, 46]. In p-type Sm doped ZnO thin films [6], ferromagnetism has been reported for 5 to 17 at.% Sm doped ZnO with maximum magnetization of approximately 2.5×10^{-5} emu, with paramagnetic behavior at Sm concentration below 5 at%, undoped ZnO being diamagnetic. The defects play a crucial role in origin of magnetic behavior of ZnO [38].

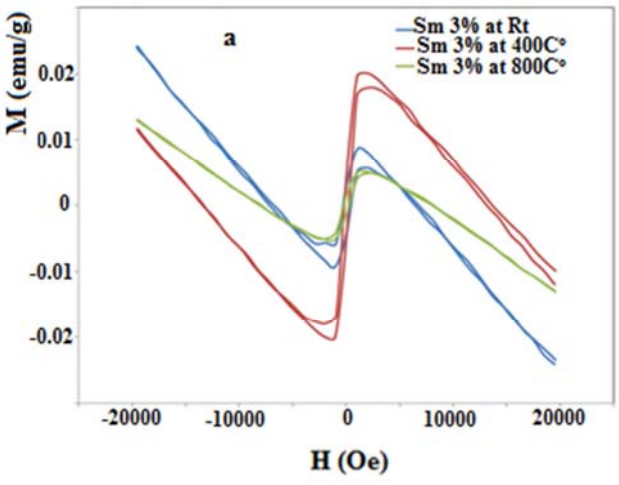

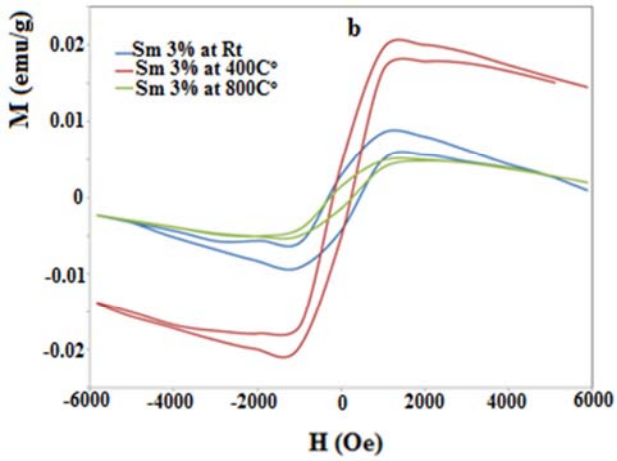

Figure 10. *Hysteresis loop of $Zn_{0.97}Sm_{0.3}O$ at RT, 400 and 800°C measured at RT with magnetic field at a) 20000Oe and b) at 6000Oe.*

Table 2. *Magnetic parameters H_C(Oe), M_S(emu/g) and M_r(emu/g) for ZnO and ZnO:Sm system annealed at 100, 400 and 800°C.*

At RT		
Parameter	ZnO	$Zn_{0.097}Sm_{0.03}O$
H_COe	286	1004.8
M_S emu/g	0.97327	9.15×10^{-3}
M_r emu/g	0.19919	2.97×10^{-3}
Annealing at 400°C		
Parameter	ZnO	$Zn_{0.097}Sm_{0.03}O$
H_COe	990	1004.8
M_S emu/g	2.3×10^{-3}	20×10^{-3}
M_r emu/g	1.9×10^{-3}	4.28×10^{-3}
Annealing at 800°C		
Parameter	ZnO	$Zn_{0.097}Sm_{0.03}O$
H_COe	312	1004.8
M_S emu/g	3.4×10^{-3}	5×10^{-3}
M_r emu/g	1.1×10^{-3}	1.6×1^{-3}

3.2.2. ESR

Electron spin resonance (ESR) is an effective tool to investigate the oxidation state, electronic configuration and site occupancy of the dopant transition metal ion more critically and also to understand the carrier concentration and magnetic exchange coupling at a microscopic level. As the numbers of unpaired electrons are different in different oxidation states, they can be easily distinguished from the number of fine transitions in the ESR spectra from their g-values. In addition the ESR technique is very sensitive method for detecting ferromagnetic ordering as well as other magnetic species.

A typical ESR spectrum of pure and doped ZnO at room temp are shown in Figure 11 a, b give the signales of g factor of the system. Symmetric resonance was observed for ZnO and Sm 3% doped ZnO, and the resonance shifts to a lower field, which corresponds to the increase in g-value. The obvious resonance at around g = 1.96 ± 0.002 (g = 1.958 for pure ZnO and g= 1.962 for Sm 3% doped ZnO) is observed. The resonance at g = 1.960 is attributed to shallow donors, normally, small donor centers are introduced by some defects or impurities in ZnO [6, 47-49]. For pure ZnO, there is no resonance at The position at g = 1.994 which generally attributed to singly ionized oxygen vacancies. In addition, it

can be seen that whit doping 3% sm g = 1.960. Therefore, 3% Sm doping may introduce extra ESR resonance, which may be from Sm doping induced shallow donors. The high g resonance suggests the ferromagnetic ordering or strong exchange coupling of the magnetic ions. Although the origin of the signal with these g-values are still unclear, it has been demonstrated in the literature that the paramagnetic signal around g value of 1.96 appears often owing to residual impurities in ZnO as well as intrinsic defects like oxygen vacancies or Zn interstitial [6, 50-56].

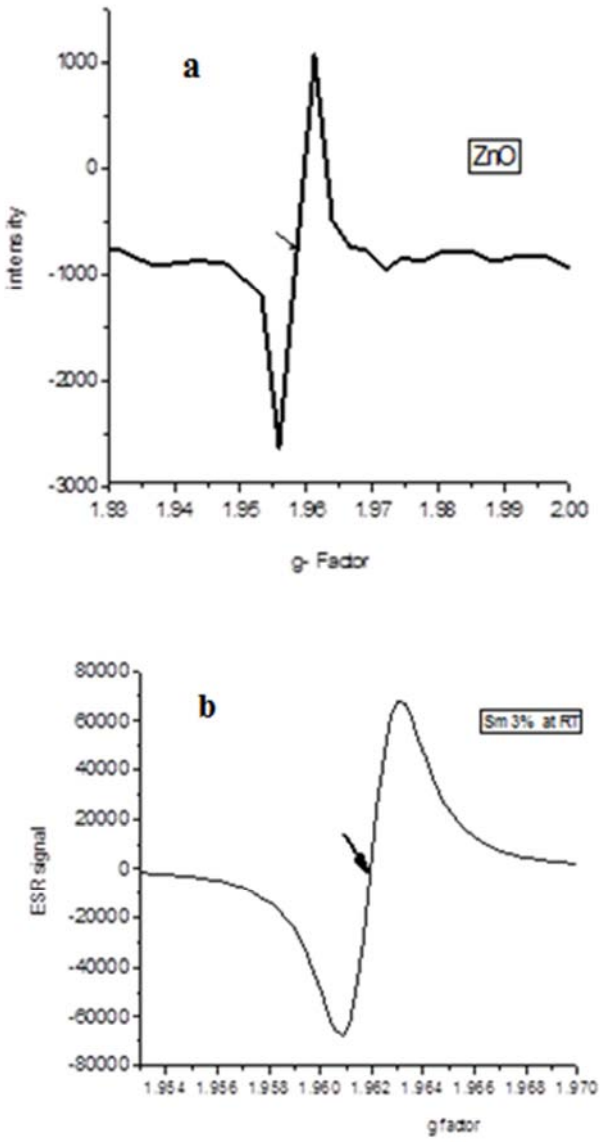

Figure 11. *G-factor signals for ZnO and ZnO doped 3% Sm at room temperature.*

4. Conclusions

We have successfully synthesized Sm doped ZnO nanoparticles with 3% concentrations by coprecipitation method. The XRD pattern of all the samples showed ZnO hexagonal wurtzite structure with sharp and intense peaks with small change in lattice parameters due to Sm doping in ZnO, indicating the substitution of Sm ions for Zn sites. Magnetic measurements show an enhancement in room temperature ferromagnetism (RTFM) with Sm doping. Ferromagnetic behavior exists over and above the diamagnetic behavior. Undoped ZnO show super ferromagnetic related to Zn vacancies, with doping the oxygen vacancies favored in formation than Zn vacancies so the general behavior is diamagnetic.

References

[1] A. Wei, L. Pan, W. Huang, Materials Science and Engineering B 176 (2011) 1409.

[2] Z. L. Wang, Adv. Funct. Mater. 18 (2008) 3553.

[3] D. A. Arora, K. Asokan, A. Mahajan, RSC Adv. 6 (2016) 78122.

[4] Y. Liu, W. Luo, R. Li, H. Zhu, X. Chen, Opt. Express 17:12 (2009) 9748.

[5] B. Roy, S. Chakrabarty, O. Mondal, M. Pal, A. Dutta, Mater. Charact., 70 (2012) 1.

[6] J. Piao, L. Tseng, J. Yi, Chemical Physics Letters 649 (2016) 19.

[7] T. Dietl, H. Ohno, F. Matsukura, J. Cibert, D. Ferrand, Science 287 (2000) 1019.

[8] B. D. Yuhas, D. O. Zitoun, P. J. Pauzauskie, Angew. Chem. Int. Ed. 45 (2006) 420.

[9] A. J. Kulandaisamy, Ceramics International (2015) (http://dx.doi.org/10.1016/j.ceramint.2015.09.084).

[10] B. Pal, S. Dhara, P. K. Giri, Journal of Alloys and Compounds (2014), doi: (http://dx.doi.org/10.1016/j.jallcom.2014.06.087).

[11] G. Shen, J. H. Cho, S. Jung, and C. J. Lee, Chem. Phys. Lett. 401 (2005) 529.

[12] G. Vijayaprasath, R. Murugan, Ceramics International, (http://dx.doi.org /10.1016/ j.cer amint. 2015.04.160).

[13] J. S. Ruiz, G. Criado, M. H. Chu, Nano Lett., 11 (2011) 5322.

[14] W. An, X. Wu, X. C. Zeng, J. Phys. Chem. C, 112 (2008) 5747.

[15] S. Dhar, O. Brandt, M. Ramsteiner, Phys. Rev. Lett., 94 (2005) 037205.

[16] D. Wang, Q. Chen, G. Xing, Nano Letters, 12 (2012) 3994.

[17] G. Vijayaprasath, G. Ravi, A. S. Haja Hameed, J. Phys. Chem. C, 118 (2014) 9715.

[18] B. M Abdolmajid, Int. J. Electrochem. Sci; 4 (2009) 247.

[19] Renugadevi et al., IJPSR 3:8 (2012) 2639.

[20] D. Gao, Z. Zhang, J. Fu, Journal of applied physics 105 (2009) 113928.

[21] N. H. Hong, J. Sakai, N. Poirot, Phys. Rev. B 73 (2006) 132404.

[22] S. Banerjee, M. Mandal, N. Gayathri, Appl. Phys. Lett. 91 (2007) 182501.

[23] A. Sundaresan, R. Bhargavi, N. Rangarajan, Phys. Rev. B 74 (2006) 161306.

[24] N. H. Hong, J. Sakai, and V. Briz'e, J. Phys.: Condens. Matter 19 (2007) 036219.

[25] A. Sundaresan, R. Bhargavi, Phy Rev B; 74 (2006) 161306.

[26] S. Kumar, Y. J. Kim, B. H. Koo, Materials Letters 63:2 (2009) 194.

[27] Q. Wang, Q. Sun, G. Chen, Phy Rev B 77 (2008) 205411.

[28] A. Zubiaga, F. Plazaola, Phys. Rev. B 76 (2007) 085202.

[29] N. Rajamanickam, Journal of Alloys and Compounds 614 (2014) 151.

[30] D. Y. Inamdar, A. D. Lad, J. Phys. Chem. C 114 (3) (2010) 1451.

[31] A. Sundaresan, R. Bhargavi, Phys. Rev. B 74 (2006) 161306.

[32] R. N. Aljawfi, F. Rahman, Materials Letters 99 (2013) 18.

[33] Y. Wang, Materials Research Bulletin 83 (2016) 408.

[34] J. B. Yi, C. C. Lim, G. Z. Xing, Phys Rev Lett. 104:13 (2010) 137201.

[35] Y. Wang, X. Luo, Chem Mater. 27:4 (2015) 1285.

[36] Y. Wang, J. Piao, G. Xing, Y. Lu, Journal of Materials Chemistry C (2015).

[37] A. G. El Hachimi, H. Zaari, A. Benyoussef, Journal of rare earths 32: 8 (2014) 715.

[38] S. Chawla, M. Saroha, R. K. Kotnala, Electron. Mater. Lett. 10: 1 (2014) 73.

[39] U. Ozgur, Ya. I. Alivov, C. Liu, J. Appl. Phys. 98 (2005) 041301.

[40] X. S. Wang, Z. C. Wu, J. F. Webb, Appl Phys. A 77 (2003) 561.

[41] S. J. Pearton, C. R. Abernathy, J. Appl. Phys. 93 (2003) 1.

[42] J. M. D. Coye, M. Venkatesan, and, Nature Materials 4 (2005) 173.

[43] T. Dietl, H. Ohno, F. Matsukura, Science 287 (2000) 1019.

[44] K. Jayanthi, S. Chawla, A. Joshi, J. Phys. Chem. C. 114 (2010) 18429.

[45] S. Chawla, K. Jayanthi, Phys. Rev. B 79 (2009) 125204.

[46] S. Chawla, K. Jayanthi, J. Appl. Phys. 10 6 (2009 113923.

[47] A. Janotti, C. G. V. d. Walle, Phys. Rev. B 76 (2007) 165202.

[48] N. Y. Garces, et al., Appl. Phys. Lett. 80 (2002) 1334.

[49] I. Zutic, J. Fabian, S. C. Erwin, IBM J. Res. Dev. 50 (2006) 121.

[50] T. Tsuji, Y. Terai, M. Kamarudin, 358 (2012) 2443.

[51] T. Ishizuka, Anal. Chem. 45 (1973) 538.

[52] W. M. Jadwisienczak, H. J. Lozykowski, A. J. Electron. Mater. 31 (2002) 776.

[53] X. Q. Meng, J. Lumin. 122 (2007) 766.

[54] K. Samanta, P. Bhattacharya, R. S. Katiyar, Appl. Phys. Lett. 87 (2005) 101903.

[55] H. Y. He, J. Fei, J. Lu, J. Nanostruct. Chem. 5 (2015) 169.

[56] L. T. Tseng, et al., AIP Adv. 4 (2014) 067117.